

# Journal of Materials Chemistry A

Accepted Manuscript



This is an *Accepted Manuscript*, which has been through the Royal Society of Chemistry peer review process and has been accepted for publication.

*Accepted Manuscripts* are published online shortly after acceptance, before technical editing, formatting and proof reading. Using this free service, authors can make their results available to the community, in citable form, before we publish the edited article. We will replace this *Accepted Manuscript* with the edited and formatted *Advance Article* as soon as it is available.

You can find more information about *Accepted Manuscripts* in the [Information for Authors](#).

Please note that technical editing may introduce minor changes to the text and/or graphics, which may alter content. The journal's standard [Terms & Conditions](#) and the [Ethical guidelines](#) still apply. In no event shall the Royal Society of Chemistry be held responsible for any errors or omissions in this *Accepted Manuscript* or any consequences arising from the use of any information it contains.



## High-voltage poly(methylethyl $\alpha$ -cyanoacrylate) composite polymer electrolyte for 5 V lithium batteries

Received 00th January 20xx,  
Accepted 00th January 20xx

DOI: 10.1039/x0xx00000x

www.rsc.org/

Jingchao Chai<sup>a,b,†</sup>, Jianjun Zhang<sup>a,b,‡</sup>, Pu Hu<sup>a,b</sup>, Jun Ma<sup>a</sup>, Huiping Du<sup>a,b</sup>, Liping Yue<sup>a</sup>, Jianghui Zhao<sup>a</sup>, Huijie Wen<sup>a</sup>, Zhihong Liu<sup>a</sup>, Guanglei Cui<sup>a,\*</sup> and Liquan Chen<sup>c</sup>

High-voltage lithium batteries have attracted increasing attention for large scale energy storage application in electrical vehicles, smart grids and other electronic devices. However, a major bottleneck to achieve high-voltage lithium batteries is the anodic voltage stability of electrolytes. Herein, we fabricate a composite polymer electrolyte, comprised of poly(methylethyl  $\alpha$ -cyanoacrylate), polytetrafluoroethylene nonwoven and lithium bis(oxalate) borate salt. The composite polymer electrolyte presents a wide electrochemical window, which is explored to address the above-mentioned bottleneck. It is demonstrated that such composite polymer electrolyte exhibits higher ionic conductivity ( $1.24 \text{ mS cm}^{-1}$  at  $25^\circ\text{C}$ ), better dimensionally thermal resistance ( $150^\circ\text{C}$ ) and higher ion transference number (0.63) compared to those of commercial available liquid electrolyte with polypropylene separator. In addition,  $\text{LiNi}_{0.5}\text{Mn}_{1.5}\text{O}_4/\text{Li}$  batteries employing such composite polymer electrolyte deliver excellent cycling performance and outstanding rate capability. So, it is demonstrated that poly(methylethyl  $\alpha$ -cyanoacrylate) based polymer electrolyte appears to be a promising candidate of high-voltage lithium batteries electrolyte towards next generation high energy density batteries.

### Introduction

With rapid development of electrical vehicles, smart grids and other electronic devices, high-voltage lithium batteries have been a focus in the current energy storage research due to their promise in energy density batteries.<sup>1, 2</sup> To further increase the energy density, tremendous attention has been paid to increase specific capacity and discharge voltage of the cathode materials.<sup>3, 4</sup> However, conventional carbonate based liquid electrolytes decompose readily when the cell is charged over  $4.5 \text{ V}$ .<sup>5</sup> Therefore, the demand for a high-voltage tolerant electrolyte has become a high priority for the development of lithium batteries with high energy density. Compared with commercially available liquid electrolytes, polymer electrolyte is regarded as an effective solution to the above-mentioned issues because of their good electrochemical and interfacial compatibility.<sup>6</sup> Solid polymer electrolyte, one of the most promising polymer electrolyte, may be a potential candidate to solve this problem, but the lower ionic conductivity at ambient temperature limits its future application in electrical vehicles.<sup>7, 8</sup> Gel polymer electrolyte, consisted of liquid electrolyte which is immobilized in a polymer matrix, suffers from an inferior mechanical performance.<sup>9-11</sup> Furthermore, the

performance of currently available pristine polymer electrolyte cannot meet the overall requirements of commercial lithium ion batteries. Therefore, it is essential to open up a novel group of composite polymer electrolyte with excellent mechanical strength, superior heat resistance, enlarged electrochemical window and high ionic conductivity.

It is well known that polytetrafluoroethylene (PTFE) is a synthetic fluoropolymer of tetrafluoroethylene. Due to its superior thermostability and chemical stability, PTFE has been widely applied in many areas.<sup>12-14</sup> In present, PTFE nonwoven is regarded as an ideal polymer matrix to develop advanced separator with excellent comprehensive properties. However, it is difficult for conventional liquid electrolyte to penetrate into the interspace of PTFE nonwoven, because of the low surface energy groups ( $-\text{CF}_2-$ ).<sup>14, 15</sup> Cyanoacrylate, known as a kind of stable adhesive, has been used in energy storage system.<sup>16-19</sup> In our group, Hu et. al developed a novel poly(ethyl  $\alpha$ -cyanoacrylate) gel polymer electrolyte, which remarkably improved the cycling performance of  $\text{LiMn}_2\text{O}_4$ -based batteries, especially at elevated temperatures.<sup>19</sup> Inspired by the better chemical stability of isopropyl than ethyl, we try to modify PTFE nonwoven with poly(methylethyl  $\alpha$ -cyanoacrylate) (PMCA) to achieve a novel composite polymer electrolyte to well match with 5 V-class cathode. It is speculated that such composite polymer electrolyte could possess superior electrochemical stability, good electrolyte wettability and high ionic conductivity, resulting in an improved electrochemical performance of high-voltage lithium batteries.

To date, there is no report on PTFE nonwoven supported PMCA based polymer electrolyte for 5 V high-voltage lithium batteries. In this work, we demonstrate the feasibility to realize stable cycling performance of 5 V-class polymer lithium battery

<sup>a</sup> Qingdao Industrial Energy Storage Technology Institute, Qingdao Institute of Bioenergy and Bioprocess Technology, Chinese Academy of Sciences, Qingdao 266101, P. R. China. E-mail: cuigl@qibebt.ac.cn

<sup>b</sup> University of Chinese Academy of Sciences, Beijing 100049, P. R. China.

<sup>c</sup> Beijing National Laboratory for Condensed Matter Physics, Institute of Physics, Chinese Academy of Sciences, Beijing 100190, P. R. China.

<sup>†</sup> These authors contributed equally to this work.

<sup>‡</sup> Electronic Supplementary Information (ESI) available: [details of any supplementary information available should be included here]. See DOI: 10.1039/x0xx00000x

## PAPER

for the first time. Lithium nickel manganese oxide ( $\text{LiNi}_{0.5}\text{Mn}_{1.5}\text{O}_4$ )-based cells with this polymer electrolyte present good performance in both rate capability and galvanostatic cycling performance, which confirms its potential application in high-voltage rechargeable lithium batteries with enhanced safety and high energy.

## Results and discussion

Schematic illustration for the preparation of composite polymer electrolyte based on polytetrafluoroethylene supported poly(methylethyl  $\alpha$ -cyanoacrylate) is displayed in the ESI, † (Fig. S1). 5.0 g methylethyl  $\alpha$ -cyanoacrylate (MCA) and 1.0 g lithium bis(oxalate)borate (LiBOB) are dissolved into 100 g absolute acetone and stirred for 10 hrs. Then, PTFE nonwoven is immersed in the as-obtained solution for 10 mins and then put into a dry workshop (with a humidity of 30 % at 25 °C) for 30 mins to form composite polymer electrolyte. The water molecule in dry workshop acts as the initiator for polymerization of PMCA. Then, the resultant PTFE-PMCA-LiBOB composite membrane (hereafter abbreviated as “composite membrane”) is dried in vacuum oven at 60 °C for 24 hrs. Composite membrane is saturated in PC containing 1 M LiBOB for 30 mins and the gel composite polymer electrolyte (hereafter abbreviated as “PFCA-CPE”) is obtained.

Typical SEM images of PP separator (Celgard 2500), PTFE nonwoven and composite membrane are demonstrated in Fig. 1. As shown in Fig. 1a, the commercialized PP separator, which is prepared by uniaxial stretching process,<sup>20</sup> has a typical slit-like pore structure. It is obviously observed in Fig. 1b that PTFE nonwoven possesses a three-dimensional porous network structure with diameters ranging from 0.2  $\mu\text{m}$  to 0.6  $\mu\text{m}$ . After the incorporation of PMCA on PTFE nonwoven (shown in Fig. 1c), the obtained composite membrane presents a compact morphology. Aforementioned structure is favorable to suppress the growth of lithium dendrites and self-discharging, which is significantly advantageous to improve battery safety. Absorption peak of composite membrane at 2987, 2942 ( $\nu_{\text{CH}_3, \text{CH}_2}$ ), 2248

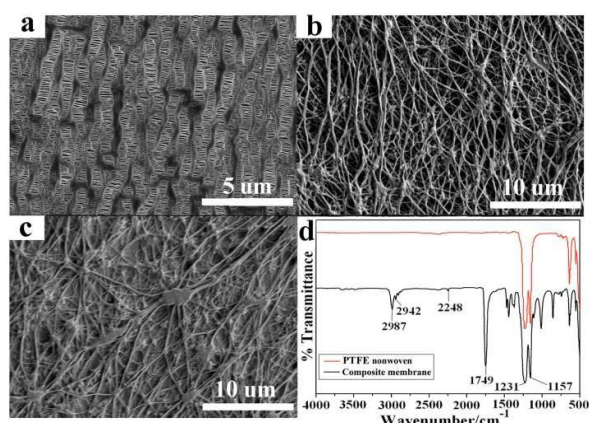


Fig. 1 Typical SEM images of PP separator (a), PTFE nonwoven (b), and composite membrane (c) and (d) FTIR spectra of composite membrane and PTFE nonwoven.

## Journal of Materials Chemistry A

( $\nu_{\text{C=N}}$ ), 1749( $\nu_{\text{C=O}}$ ) is a powerful evidence that PMCA has been successfully incorporated onto PTFE nonwoven (shown in Fig. 1d).

Mechanical strength is an important parameter for polymer electrolyte used in lithium ion batteries. Stress-strain curves display the mechanical properties of PTFE nonwoven, composite membrane and PFCA-CPE (see ESI, † Fig. S2). Both composite membrane (23.8 MPa) and PFCA-CPE (21.1 MPa) present a better mechanical property than PTFE nonwoven (18.5 MPa). There are two aspects to explain the phenomenon. Firstly, as a crystalline material, PTFE nonwoven can be a frame matrix, which could sustain the basic morphology of PFCA-CPE. Secondly, PMCA fills in the pores of PTFE nonwoven, which can form similar-reinforced concrete structures.<sup>21</sup> Aside from mechanical strength, the thickness, porosity, air permeability, electrolyte uptake and ionic conductivity of PP separator, PTFE nonwoven and composite membrane at 30 °C are listed in ESI, † (Table S1). The Gurley value of PTFE nonwoven is 50 s, which is much less than that of the PP separator (600 s). By compositing PMCA to PTFE, the Gurley value of the composite membrane has increased to more than 8000 s, which is corresponding with SEM result. In addition, thermal shrinkage properties and DSC curves for PP separator, PTFE nonwoven and composite membrane indicates that this kind of composite membrane has an excellent heat resistance (see ESI, † Fig. S3 and Fig. S4).

The amorphous degree is crucial for ionic conductivity of polymer electrolyte. As we know, the cation transport takes place in the amorphous region of polymer electrolyte.<sup>22</sup> The transport of lithium ions is assisted by the motion of chain segment. XRD patterns of the PTFE nonwoven, PMCA, composite membrane and PFCA-CPE can be seen in the ESI, † (Fig. S5). The XRD spectrum for the PTFE nonwoven exhibits spectral features similar to those of the pressed PTFE powder material.<sup>23</sup> For PTFE nonwoven, the presence of the intense peak in the XRD spectra is assigned to (100). While, PMCA would not affect the diffraction peak of PFCA-CPE, which means that PMCA is a kind of amorphous material. The amorphous PMCA in PFCA-CPE can be an appropriate medium for cationic transport.

It has been reported that the liquid electrolyte uptake would significantly affect the resistance of cells.<sup>24-26</sup> The liquid electrolyte uptake is measured by immersing the membranes into PC-based electrolyte for 10 hrs. It is determined by following equation:  $\text{EU} = [(W - W_0)/W_0] \times 100\%$ ,<sup>27</sup> where  $W_0$  and  $W$  indicated the membranes weight before and after liquid electrolyte absorption, respectively. The extra solution at the surface of the membranes is wiped with a filter paper before measuring the weight. For PP separators, the PC-based electrolyte uptake is 100 %. The electrolyte uptake of PTFE nonwoven is only 69 %, which is caused by the poor wettability of PTFE.<sup>28</sup> However, the electrolyte uptake of the composite membrane would remarkably increase to 181 % after incorporating PMCA, which is owing to the swelling of PMCA when absorbing liquid electrolyte.

Electrochemical stability of polymer electrolyte is vital for practical battery applications.<sup>29</sup> In order to contrast with traditional liquid electrolyte, a series of cells, which are assembled with different electrolyte, are tested by linear sweep voltammetry measurement. As can be seen from Fig. 2a, LiBOB-PC based

liquid electrolyte (hereafter abbreviated as “LE”) would decompose above 5.0 V. The wide electrochemical window of LiBOB-PC is due to the high electrochemical oxidation stability of LiBOB and PC. While, it is worth noting that PFCA-CPE shows a slight improvement to LiBOB-PC based liquid electrolyte, which means that this novel PFCA-CPE has a great endurance capacity to high voltage. These results indicate that PFCA-CPE can be a potential candidate for high-voltage lithium batteries polymer electrolyte.

A detailed electrochemical characterization is performed to demonstrate the feasibility of PFCA-CPE. The ionic conductivity defines how fast the energy could be released. As shown in Fig. 2b, at 25 °C, the obtained ionic conductivity of LE using PP separator and PFCA-CPE, is evaluated to be 0.57 and 1.24 mS cm<sup>-1</sup> respectively. It is noted that, the conductivity of PFCA-CPE is better than that of LE owing to the favourable interaction between lithium salt and polymer besides the increased electrolyte uptake of the PFCA-CPE. It is noted that, both ester and cyan groups with strong electron withdrawing capability are beneficial for the dissociation of the electrolytic salt, leading to a high ionic conductivity of polymer electrolyte.<sup>19</sup> Furthermore, it is found that the ionic conductivity of PFCA-CPE is higher than that of LE in a wide temperature range, which is vital for improving comprehensive performances of as-assembled lithium batteries. It is generally accepted that the ionic conductivity of liquid electrolyte using polyolefin separator is described by the Arrhenius equation (1) and the ionic conductivity of polymer electrolyte is better described by the Vogel-Tamman-Fulcher (VTF) empirical equation (2), which indicates the relationship between the ionic conductivity and the polymer chains dynamics.<sup>30</sup>

$$\sigma(T) = A \exp(-E_a/RT) \quad (1)$$

$$\sigma(T) = A T^{-1/2} \exp(-E_a/R(T-T_0)) \quad (2)$$

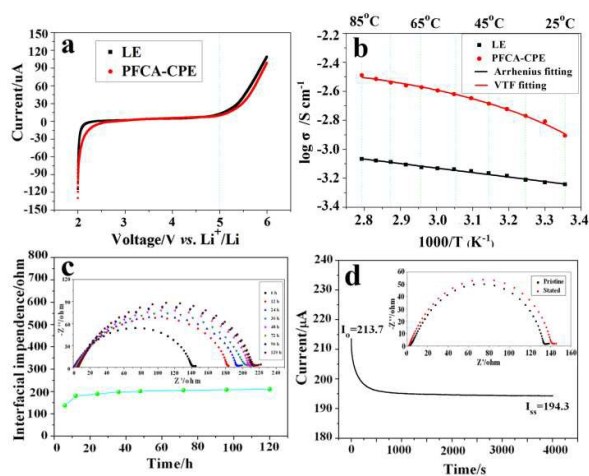


Fig. 2. a) Linear sweep voltammograms and b) ionic conductivity comparison for LE and PFCA-CPE. c) Time evolution of the interfacial resistance under open circuit conditions. The inset is corresponding EIS Nyquist plots. d) Current-time curve following a DC polarization of 0.030 V of PFCA-CPE. Insets were Nyquist profiles of the cell electrochemical impedance spectroscopy response before and after polarization.

Where A is pre-exponential factor,  $E_a$  is the activation energy,  $T_0$  is a temperature correlated to the glass transition temperature, and R is the ideal gas constant. The fitting results are shown in the ESI, † (Table. S2). It can be easily found that PFCA-CPE has a much lower activation energy than liquid electrolyte, which is due to the low energy barrier for lithium ion transfer in PFCA-CPE.

Another vital important parameter for lithium ion batteries is interfacial stability of lithium anode. In Fig. 2c, the interface impedance initially increase, then reaches to a stable value of 200 ohm, thus suggesting good stability of the solid electrolyte interface upon long storage in contact with lithium metal. The stable interface would enhance the capacity retention of lithium ion batteries during charging/discharging process, which is vital for cycle life of batteries.

Lithium ion transference number ( $t_{Li^+}$ ) is an important parameter to rate polymer electrolyte, because the transference of lithium ions plays a decisive role during the process of charging and discharging of lithium ion batteries. As seen from Fig. 2d, polarization makes the interfacial resistance change from 130 ohm to 138 ohm for PFCA-CPE. In addition, the current value reaches a plateau of 194.3  $\mu$ A from the initial current values of 213.7  $\mu$ A. So, from Bruce-Vincent equation, we could easily get the  $t_{Li^+}$ , about 0.63 for PFCA-CPE. While, the value for LE is only 0.31 (see ESI, † Fig. S6). In our case, the lithium ion transference number of PFCA-CPE is larger than that of previously reported LiPF<sub>6</sub>/PVdF and LiPF<sub>6</sub>/PAN, where the calculated value are 0.24<sup>31</sup> and 0.44,<sup>32</sup> respectively. The high  $t_{Li^+}$  values of the PFCA-CPE may be owing to the formation of BOB<sup>-</sup>...( $\delta^+$ )C=C=N( $\delta^-$ ) or BOB<sup>-</sup>...( $\delta^+$ )C=C=O( $\delta^-$ ) complexes in the polymer matrices, resulting in the fixation of the BOB<sup>-</sup> anion, which benefits to improve the  $t_{Li^+}$  value of PFCA-CPE.<sup>33</sup> In addition, PMCA polymer electrolyte delivered a high lithium transference numbers (0.504). While, liquid electrolyte using PTFE nonwoven has a lower value (0.329). It should be noticed that both the values of PMCA polymer electrolyte and liquid electrolyte using PTFE nonwoven are lower than that of PFCA-CPE. Synergistic reaction between PTFE and PMCA would increase the lithium transference numbers of polymer electrolyte. The large lithium ion transference number would generate low concentration gradients, which can endow the as-assembled batteries better power capability and higher peak-power densities.<sup>34</sup>

As is known, high energy density lithium ion batteries favor to improve the endurance of electric vehicles.<sup>35-37</sup> The available energy stored in a fully charged cell depends on the discharge current  $I_{dis}$  and V:  $\text{energy} = \int_0^{AV} I \cdot V(t) dt$ .<sup>38</sup> LiNi<sub>0.5</sub>Mn<sub>1.5</sub>O<sub>4</sub> is a kind of cathode with high-voltage up to 5.0 V (0.6 V higher than LiCoO<sub>2</sub>, see ESI, † Fig. S7 and Fig. S8), endowing the corresponding batteries with higher energy. While, whether polymer electrolyte can be available in practical applications depends on its durable rate capability in lithium ion battery.<sup>29, 39, 40</sup> The rate capability of LE and PFCA-CPE in LiNi<sub>0.5</sub>Mn<sub>1.5</sub>O<sub>4</sub>/Li cells are compared in Fig. 3a. The cell with PFCA-CPE at the current density of 0.2 C presents an initial discharge capacity of 142.8 mAh g<sup>-1</sup> and retains 65.2 mAh g<sup>-1</sup> at 10.0 C, while that of LE cells is only 23.2 mAh g<sup>-1</sup> at 10.0 C. Fig. 3b depicts the typical charge/discharge performance of LiNi<sub>0.5</sub>Mn<sub>1.5</sub>O<sub>4</sub>/Li cells using PFCA-CPE at varied rates. As shown in Fig. 3b, from 0.2 C to 10.0

## PAPER

C,  $\text{LiNi}_{0.5}\text{Mn}_{1.5}\text{O}_4/\text{Li}$  cells show a typical voltage plateau at 4.7 V, which is due to the  $\text{Ni}^{2+}/\text{Ni}^{4+}$  redox reaction. Additionally, discharge voltage plateau decreases slowly but still keeps relatively high values with the increasing discharge rate. The result indicates that the as-developed PFCA-CPE exhibits considerable rate capability for the high-voltage lithium ion battery. The acceptable rate capability can be ascribed to the high lithium ionic conductivity and good interfacial compatibility of the PFCA-CPE.<sup>10</sup> Hence, PFCA-CPE presents a satisfactory rate performance between 0.2 C and 10.0 C, which is significant to high energy power batteries.

Ragone plot describes the relationship between gravimetric energy and power density of  $\text{LiNi}_{0.5}\text{Mn}_{1.5}\text{O}_4/\text{Li}$  cells.<sup>41-43</sup> As well known,  $\text{LiNi}_{0.5}\text{Mn}_{1.5}\text{O}_4/\text{Li}$  cells present a higher gravimetric energy density than  $\text{LiCoO}_2/\text{Li}$  cells and  $\text{LiFePO}_4/\text{Li}$  cells, as a result of the higher voltage than that of  $\text{LiCoO}_2$ <sup>44, 45</sup> and  $\text{LiFePO}_4$ .<sup>44</sup> Fig. 3c gives the Ragone plot curves which compare the performance of  $\text{LiNi}_{0.5}\text{Mn}_{1.5}\text{O}_4/\text{Li}$  cells using LE and PFCA-CPE. It is obvious that, both  $\text{LiNi}_{0.5}\text{Mn}_{1.5}\text{O}_4/\text{Li}$  cells using LE and PFCA-CPE have a higher gravimetric energy density than  $\text{LiCoO}_2/\text{Li}$  cell. The calculated output energy density of  $\text{LiNi}_{0.5}\text{Mn}_{1.5}\text{O}_4/\text{Li}$  cells using PFCA-CPE is  $670 \text{ Wh kg}^{-1}$  at a current density of 0.2 C based on the mass of active materials, which is slightly higher than the value for LE counterpart ( $650 \text{ Wh kg}^{-1}$ ). However, the PFCA-CPE based cells exhibit an appreciable higher energy density with the increasing power density. For example, at a current density of 10.0 C, the calculated output energy density of PFCA-CPE based cell can be up to  $300 \text{ Wh kg}^{-1}$  based on the mass of active materials, which is comparable to previous report.<sup>46</sup> However, the calculated output energy density

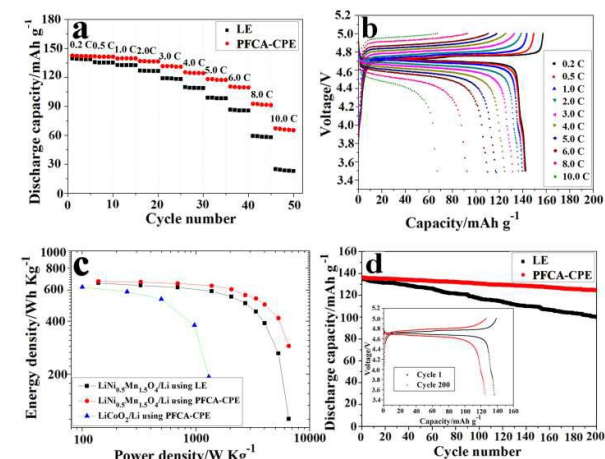


Fig. 3. a) Rate capability of  $\text{LiNi}_{0.5}\text{Mn}_{1.5}\text{O}_4/\text{Li}$  cells using LE and PFCA-CPE at 25 °C. b) Charge/discharge curves of  $\text{LiNi}_{0.5}\text{Mn}_{1.5}\text{O}_4/\text{Li}$  cells using PFCA-CPE at varied current density. c) Ragone plot comparing gravimetric energy and power density of  $\text{LiNi}_{0.5}\text{Mn}_{1.5}\text{O}_4/\text{Li}$  cells using LE and PFCA-CPE, and  $\text{LiCoO}_2/\text{Li}$  cell using PFCA-CPE, where the cell weight is determined on the basis of the weight of cathode active material. d) Discharging capacity retention of  $\text{LiNi}_{0.5}\text{Mn}_{1.5}\text{O}_4/\text{Li}$  cells using LE and PFCA-CPE at 1.0 C. Inset is the corresponding charge/ discharge curves of 1<sup>st</sup> and 200<sup>th</sup> cycles.

## Journal of Materials Chemistry A

of LE-based cell is only  $110 \text{ Wh kg}^{-1}$  at this rate. It means that, the calculated output energy density of PFCA-CPE based cell is about three times higher than that of LE-based counterpart cell at the high rate of 10.0 C. It may be attributed to the faster transport rate of lithium ion in PFCA-CPE and more compatible interface between electrode and PFCA-CPE.

In order to improve cyclability of the  $\text{LiNi}_{0.5}\text{Mn}_{1.5}\text{O}_4$  based batteries, much effort has been put on  $\text{LiNi}_{0.5}\text{Mn}_{1.5}\text{O}_4$  electrode such as replacing small amounts of manganese or nickel with other metal ions with a valence of +3,<sup>47-49</sup> and surface modification of  $\text{LiNi}_{0.5}\text{Mn}_{1.5}\text{O}_4$ .<sup>50, 51</sup> Lee et. al have used a polyimide-coated  $\text{LiNi}_{0.5}\text{Mn}_{1.5}\text{O}_4$  electrode for 5 V-class batteries.<sup>50</sup> The wrapping layer could protect liquid electrolyte from direct contact to  $\text{LiNi}_{0.5}\text{Mn}_{1.5}\text{O}_4$  electrode, thus suppress the decomposition of liquid electrolyte occurring on the surface of  $\text{LiNi}_{0.5}\text{Mn}_{1.5}\text{O}_4$ . A capacity retention (after 100<sup>th</sup> cycle) of polyimide-coated  $\text{LiNi}_{0.5}\text{Mn}_{1.5}\text{O}_4$  was found to be 93.2 % at room temperature. To investigate the viability of PFCA-CPE for high-voltage lithium batteries, cycle performance of  $\text{LiNi}_{0.5}\text{Mn}_{1.5}\text{O}_4/\text{Li}$  cells using LE and PFCA-CPE is depicted in Fig. 3d. The first discharge capacity of PFCA-CPE based cell is  $137.2 \text{ mAh g}^{-1}$ , higher than that of LE-based cell ( $134.5 \text{ mAh g}^{-1}$ ). In particular, the PFCA-CPE based cells present an excellent discharge capacity retention. After 100 charge/discharge cycles, PFCA-CPE based  $\text{LiNi}_{0.5}\text{Mn}_{1.5}\text{O}_4/\text{Li}$  cells possess a better discharge capacity retention, which can be up to  $130.6 \text{ mAh g}^{-1}$  (about 95.8 % of the first discharge capacity), which is better than previous work.<sup>50, 52</sup> In addition, the PFCA-CPE based  $\text{LiNi}_{0.5}\text{Mn}_{1.5}\text{O}_4/\text{Li}$  cells display about 8.5 % capacity loss after 200 cycles (from  $136.2 \text{ mAh g}^{-1}$  to  $124.6 \text{ mAh g}^{-1}$ ) with a slight increase of polarization according to the corresponding charge/ discharge curves in Fig. 3d. In a sharp contrast, of this kind of cells is observed to be  $100.1 \text{ mAh g}^{-1}$  after 200 cycles, corresponding to 74.4 % of capacity retention, which may be due to the decomposition of liquid electrolyte. Considering the state of art performance of  $\text{LiNi}_{0.5}\text{Mn}_{1.5}\text{O}_4/\text{Li}$  batteries, PFCA-CPE is a fantastic polymer electrolyte for well matching with 5 V-cathode.

Fig. 4 shows typical SEM image comparison of  $\text{LiNi}_{0.5}\text{Mn}_{1.5}\text{O}_4$  cathode after 200 cycles. By comparison of SEM images of  $\text{LiNi}_{0.5}\text{Mn}_{1.5}\text{O}_4$  cathode before and after charge/discharge cycles (see ESI, † Fig. S9), it is easy to find a PMCA wrapping layer onto the  $\text{LiNi}_{0.5}\text{Mn}_{1.5}\text{O}_4$  cathode. Fig. 4c is schematic illustrations of PMCA wrapping layer formed on the  $\text{LiNi}_{0.5}\text{Mn}_{1.5}\text{O}_4$  cathode. There are two significant factors which can affect the performance of the high-voltage battery. On one hand, PFCA-CPE has formed a PMCA wrapping layer onto the  $\text{LiNi}_{0.5}\text{Mn}_{1.5}\text{O}_4$  cathode, which functions as an ion-conductive protection skin to suppress the undesired interfacial side reactions. On the other hand, the PECA wrapping layer can inhibit the dissolution and transference of  $\text{Mn}^{3+}$  ions.<sup>[13]</sup>

To further investigate the viability of PFCA-CPE,  $\text{LiNi}_{0.5}\text{Mn}_{1.5}\text{O}_4/\text{graphite}$  full cells are assembled with PFCA-CPE. The full cells are tested at a current density of 0.5 C between the voltage range of 3.5 V and 4.9 V at 25 °C. The results are shown in Fig. 5a and Fig. 5b. The reversible capacity of full cells increase to about  $118 \text{ mAh g}^{-1}$  after few cycles with an observed discharge

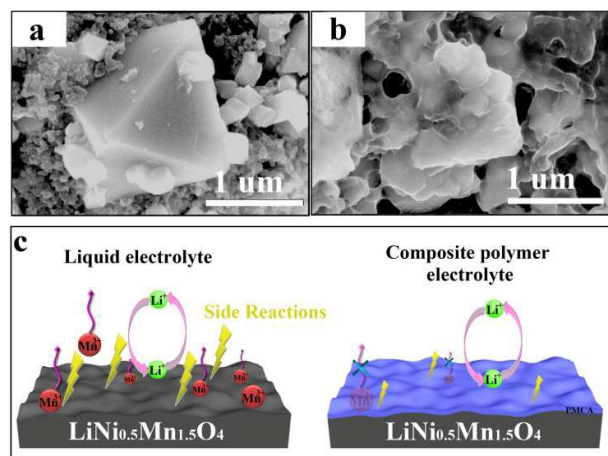


Fig. 4. Typical SEM images of  $\text{LiNi}_{0.5}\text{Mn}_{1.5}\text{O}_4$  cathode after 200 cycle of the batteries using LE a) and PFCA-CPE b). Insets showed the magnified patterns. c) Schematic illustrations of PMCA wrapping layer formed on the  $\text{LiNi}_{0.5}\text{Mn}_{1.5}\text{O}_4$  cathode.

plateau. The capacity retention is as high as 91.5 % even after 100 cycles, suggesting the electrochemical stability of PFCA-CPE. The charge/discharge rate capacity of  $\text{LiNi}_{0.5}\text{Mn}_{1.5}\text{O}_4/\text{graphite}$  full cells is under further investigation as well. The first coulombic efficiency is only 91.7 % when a current density of 0.5 C is used for both charge and discharge progress. However, the coulombic efficiency slightly increases to about 99.8 % in the subsequent cycles, indicating superior stability of the electrode/electrolyte interfaces during the charge/discharge process.<sup>53</sup> In addition, as can be seen from the charge/discharge curves of  $\text{LiNi}_{0.5}\text{Mn}_{1.5}\text{O}_4/\text{graphite}$  full cells, the polarization is very small, which is due to the high ionic conductivity of PFCA-CPE.

In an effort to obtain a better understanding of the advantageous cycle performance of the PFCA-CPE based  $\text{LiNi}_{0.5}\text{Mn}_{1.5}\text{O}_4/\text{graphite}$  full cells, the AC impedance spectra of batteries at fully discharged state after the 10<sup>th</sup> cycle and the 100<sup>th</sup> cycle are analyzed in Fig. 5c. The equivalent circuit (see ESI, † Fig. S10) proposes a semicircle of impedance spectra at a high frequency range and a semicircle at the medium-to-low frequency region. It has been reported that the first semicircle is assigned to the diffusion resistance of  $\text{Li}^+$  ions through the unfavourable solid electrolyte interfacial (SEI) film deposited on the electrode ( $R_{\text{SEI}}$ ) and the second semicircle is attributed to the charge transfer resistance ( $R_{\text{ct}}$ ).<sup>50</sup> For PFCA-CPE based  $\text{LiNi}_{0.5}\text{Mn}_{1.5}\text{O}_4/\text{graphite}$  full cells,  $R_{\text{SEI}}$  increases from 18.64 ohm to 27.96 ohm and  $R_{\text{ct}}$  increases from 386.6 ohm to 484.4 ohm. It is demonstrated that the PFCA-CPE has a stable electrochemical property, which endows PFCA-CPE based  $\text{LiNi}_{0.5}\text{Mn}_{1.5}\text{O}_4/\text{graphite}$  full cells a superior cycle performance. In addition, by comparing the FTIR spectra of PFCA-CPE before and after 100 charge/discharge cycles in Fig. 5d, it can be easily found that after charge/discharge process, the absorption peak of  $\text{C}\equiv\text{N}$  change from 2248  $\text{cm}^{-1}$  to 2295  $\text{cm}^{-1}$ , and the absorption peaks of  $\text{C}=\text{O}$  changes from 1750  $\text{cm}^{-1}$  to 1789  $\text{cm}^{-1}$ , which may be due to the chelation between  $\text{Mn}^{3+}$  and PMCA. However, most of the absorption peaks of PFCA-CPE after 100 charge/discharge cycles is corresponding to

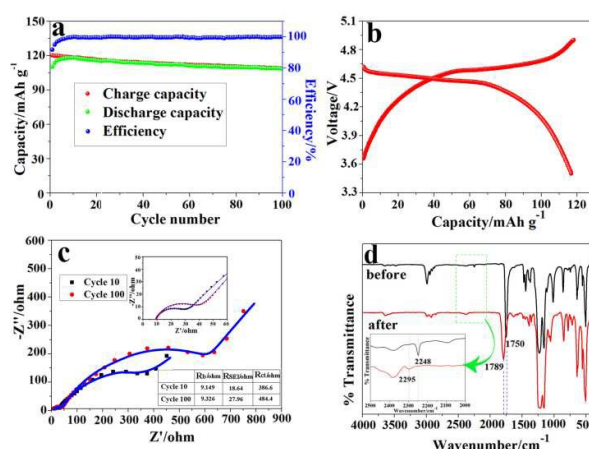


Fig. 5. a) Cycle performance and b) charge/discharge curves of  $\text{LiNi}_{0.5}\text{Mn}_{1.5}\text{O}_4/\text{graphite}$  full cells using PFCA-CPE at 0.5 C between the voltage range of 3.5 V and 4.9 V at 25 °C. c) Variation in AC impedance spectra  $\text{LiNi}_{0.5}\text{Mn}_{1.5}\text{O}_4/\text{graphite}$  full cells assembled with PFCA-CPE. d) FTIR spectra of PFCA-CPE before and after 200 charge/discharge cycles.

original PFCA-CPE. In other words, PFCA-CPE remains its excellent electrochemical stability and interfacial compatibility in  $\text{LiNi}_{0.5}\text{Mn}_{1.5}\text{O}_4/\text{graphite}$  full cells.

## Experimental

**Samples characterization:** The morphology of the samples is investigated by a field emission scanning electron microscopy (Hitachi S-4800 at 3 kV). FTIR measurements are conducted on a Fourier transform infrared spectroscopy (Bruker VERTEX 70). The Gurley value is obtained using a Gurley-type densometer (4110N, Gurley) by measuring the time of 100 cc air to pass through the membranes or separators. The porosity is measured by immersing the membranes into n-butanol for 10 hrs and calculated with the following equation:  $P = (m_b/\rho_b)/(m_b/\rho_b + m_a/\rho_a) \times 100\%$ ,<sup>39, 54</sup> where  $m_a$  and  $m_b$  are the mass of the membranes and n-butanol,  $\rho_a$  and  $\rho_b$  are the density of membranes material and n-butanol, respectively. Differential scanning calorimeter (Diamond DSC, PerkinElmer) is used to evaluate the thermal properties of the membranes. Samples are scanned from room temperature to 300 °C at a heating rate of 10 °C/min under nitrogen atmosphere. To characterize its thermal shrinkage behavior, the membranes are placed in an oven and stored at varied temperatures for 2 hrs. Thermal shrinkage ratio (TSR) is calculated according to the equation:  $\text{TSR} = [(S_0 - S)/S_0] \times 100\%$ . Here,  $S_0$  and  $S$  represent the area of the membrane before and after thermal treatment at the varied temperature for 2 hrs, respectively.

**Electrochemical evaluation:** The electrochemical stability window of PFCA-CPE is determined by a linear sweep voltammetry experiment performed on a working electrode of stainless steel and a counter electrode of lithium metal at a scan rate of 1  $\text{mV s}^{-1}$ . The ionic conductivity of LE and PFCA-CPE between two stainless steels is tested via the electrochemical impedance spectroscopy (EIS) measurement in the frequency

## PAPER

range of 1 Hz to  $10^6$  Hz. Taking into account the effects of the polarization over the electrode/electrolyte interphase, the lithium transference number ( $t_{Li^+}$ ) is calculated using the Bruce-Vincent-Evans equation:  $t_{Li^+} = [I_{ss} \times (V - I_0 R_0)] / [I_0 \times (V - I_{ss} R_{ss})]$ , where  $V$  is the applied voltage,  $I_0$  and  $I_{ss}$  are initial current and steady-state values, respectively, and  $R_0$  and  $R_{ss}$  are the initial and the steady state interfacial resistance, respectively. Current-time curve is followed by a DC polarization of 0.030 V. 2032-type coin cells are assembled by sandwiching the electrolyte between  $\text{LiNi}_{0.5}\text{Mn}_{1.5}\text{O}_4$  cathode and Li anode. In addition, lithium ion batteries are assembled with  $\text{LiNi}_{0.5}\text{Mn}_{1.5}\text{O}_4$  cathode and graphite anode. The AC impedance spectra of batteries are obtained by EIS measurements in the frequency range of 1 Hz to  $10^6$  Hz.

## Conclusions

We have successfully demonstrated PFCA-CPE to be a promising electrolyte for  $\text{LiNi}_{0.5}\text{Mn}_{1.5}\text{O}_4$  based 5 V lithium battery. The resultant PFCA-CPE shows not only higher ionic conductivity, but also superior thermal resistance and wider electrochemical window when compared with commercialized liquid electrolyte system. Crucially, the  $\text{LiNi}_{0.5}\text{Mn}_{1.5}\text{O}_4/\text{Li}$  cells using PFCA-CPE deliver superior rate capability and excellent cycle performance at varied charge/discharge current densities. The more stable electrochemical properties of PFCA-CPE endow the  $\text{LiNi}_{0.5}\text{Mn}_{1.5}\text{O}_4$  batteries a better capacity retention than liquid electrolyte. At the same time,  $\text{LiNi}_{0.5}\text{Mn}_{1.5}\text{O}_4/\text{graphite}$  full cells using PFCA-CPE at a current density of 0.5 C at 25 °C present a high discharge capacity of 118 mAh  $\text{g}^{-1}$  with an observed discharge plateau and a good capacity retention of 91.5 % even after 100 cycles. Although much deep insight work is still on the way, we believe this work represents a significant step towards high-voltage lithium batteries.

## Acknowledgements

This work is financially supported by the National Natural Science Foundation of China (Grant No. 21271180), the Strategic Priority Research Program of the Chinese Academy of Sciences (Grant No. XDA09010105), Shandong Provincial Natural Science Foundation, China (Grant No. ZR2013FZ001), the Foundation for Young Scientist in Shandong Province (Grant No. 2015BSF01021), Qingdao Institute of Bioenergy and Bioprocess Technology Director Innovation Foundation for Young Scientists. (Grant Number: QIBEBT-DIFYS-201508). Technology and Qingdao Key Lab of Solar Energy Utilization and Energy Storage Technology.

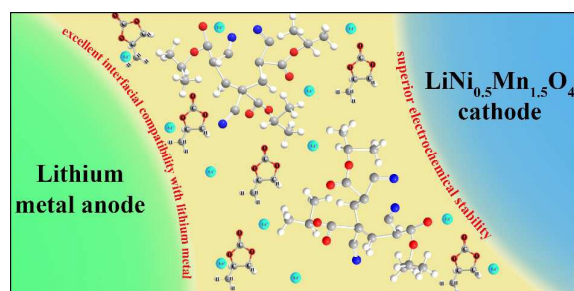
## Notes and references

1. C. K. Chan, H. Peng, G. Liu, K. McIlwrath, X. F. Zhang, R. A. Huggins and Y. Cui, *Nat. Nanotechnol.*, 2008, **3**, 31.
2. S. Wang, L. Wang, K. Zhang, Z. Zhu, Z. Tao and J. Chen, *Nano Lett.*, 2013, **13**, 4404.

## Journal of Materials Chemistry A

3. J. Xiao, X. Chen, P. V. Sushko, M. L. Sushko, L. Kovarik, J. Feng, Z. Deng, J. Zheng, G. L. Graff, Z. Nie, D. Choi, J. Liu, J. G. Zhang and M. S. Whittingham, *Adv. Mater.*, 2012, **24**, 2109.
4. A. Bhaskar, S. Krueger, V. Siozios, J. Li, S. Nowak and M. Winter, *Adv. Energy Mater.*, 2015, **5** DOI: 10.1002/aenm.201401156.
5. Z. Zhang, L. Hu, H. Wu, W. Weng, M. Koh, P. C. Redfern, L. A. Curtiss and K. Amine, *Energy Environ. Sci.*, 2013, **6**, 1806.
6. Z. Zhu, M. Hong, D. Guo, J. Shi, Z. Tao and J. Chen, *J. Am. Chem. Soc.*, 2014, **136**, 16461.
7. P. Kritzer, *J. Power Sources*, 2006, **161**, 1335.
8. E. Quartarone and P. Mustarelli, *Chem. Soc. Rev.*, 2011, **40**, 2525.
9. Y. Zhu, F. Wang, L. Liu, S. Xiao, Z. Chang and Y. Wu, *Energy Environ. Sci.*, 2013, **6**, 618.
10. P. Sun, Y. Liao, H. Xie, T. Chen, M. Rao and W. Li, *J. Power Sources*, 2014, **269**, 299.
11. J. Zhang, Z. Liu, Q. Kong, C. Zhang, S. Pang, L. Yue, X. Wang, J. Yao and G. Cui, *ACS Appl. Mat. Interfaces*, 2013, **5**, 128.
12. N. L'Heureux, S. Paquet, R. Labbe, L. Germain and F. A. Auger, *The FASEB Journal*, 1998, **12**, 47.
13. C. Bureau, J. C. Garcia Pagan, P. Ota, G. Pomier Layrargues, V. Chabbert, C. Cortez, P. Perreault, J. M. Péron, J. G. Abraldes, L. Bouchard, J. I. Bilbao, J. Bosch, H. Rousseau and J. P. Vinel, *Gastroenterology*, 2004, **126**, 469.
14. D. H. Kaelble and K. C. Uy, *J. Adhes.*, 1970, **2**, 25.
15. R. G. Chaudhuri and S. Paria, *J. Colloid Interface Sci.*, 2014, **434**, 141.
16. F. Favier, E. C. Walter, M. P. Zach, T. Benter and R. M. Penner, *Science*, 2001, **293**, 2227.
17. J. Kreuter, D. Shamenkov, V. Petrov, P. Ramge, K. Cychutek, C. Koch-Brandt and R. Alyautdin, *J. Drug Target.*, 2002, **10**, 317.
18. J. Xu, L. Zhang and G. Chen, *Sens. Actuators. B. Chem.*, 2013, **182**, 689.
19. P. Hu, Y. Duan, D. Hu, B. Qin, J. Zhang, Q. Wang, Z. Liu, G. Cui and L. Chen, *ACS Appl. Mater. Interfaces*, 2015, **7**, 4720.
20. J. Shi, T. Shen, H. Hu, Y. Xia and Z. Liu, *J. Power Sources*, 2014, **271**, 134.
21. H. A. Toutanji, *ACI Mater. J.*, 1999, **96**, 397.
22. Y. S. Zhu, X. J. Wang, Y. Y. Hou, X. W. Gao, L. L. Liu, Y. P. Wu and M. Shimizu, *Electrochim. Acta*, 2013, **87**, 113.
23. S. T. Li, E. Arenholz, J. Heitz and D. Bäuerle, *Appl. Surf. Sci.*, 1998, **125**, 17.
24. M. H. Ryou, Y. M. Lee, J. K. Park and J. W. Choi, *Adv. Mater.*, 2011, **23**, 3066.
25. K. Liu, X. Yao and L. Jiang, *Chem. Soc. Rev.*, 2010, **39**, 3240.
26. W. H. Seol, Y. M. Lee and J. K. Park, *J. Power Sources*, 2006, **163**, 247.
27. M. Yanilmaz, C. Chen and X. Zhang, *J. Polym. Sci., Part B: Polym. Phys.*, 2013, **51**, 1719.
28. S. M. M. Ramos, J. F. Dias and B. Canut, *J. Colloid Interface Sci.*, 2015, **440**, 133.
29. J. Zhang, L. Yue, Q. Kong, Z. Liu, X. Zhou, C. Zhang, Q. Xu, B. Zhang, G. Ding, B. Qin, Y. Duan, Q. Wang, J. Yao, G. Cui and L. Chen, *Sci. Rep.*, 2014, **4**, 3935.

30. F. Croce, M. L. Focarete, J. Hassoun, I. Meschini and B. Scrosati, *Energy Environ. Sci.*, 2011, **4**, 921.
31. C. Fasciani, S. Panero, J. Hassoun and B. Scrosati, *J. Power Sources*, 2015, **294**, 180.
32. Z. Zhang, G. Sui, H. Bi and X. Yang, *Journal of Membrane Science*, 2015, **492**, 77.
33. S. H. Wang, P. L. Kuo, C. T. Hsieh and H. Teng, *ACS Appl. Mat. Interfaces*, 2014, **6**, 19360.
34. M. Doyle, T. F. Fuller and J. Newman, *Electrochim. Acta*, 1994, **39**, 2073.
35. B. Kang and G. Ceder, *Nature*, 2009, **458**, 190.
36. P. Simon and Y. Gogotsi, *Nat. Mater.*, 2008, **7**, 845.
37. J. M. Tarascon and M. Armand, *Nature*, 2001, **414**, 359.
38. J. B. Goodenough and K. S. Park, *J. Am. Chem. Soc.*, 2013, **135**, 1167.
39. J. Zhang, Q. Kong, Z. Liu, S. Pang, L. Yue, J. Yao, X. Wang and G. Cui, *Solid State Ionics*, 2013, **245-246**, 49.
40. J. Zhang, L. Yue, P. Hu, Z. Liu, B. Qin, B. Zhang, Q. Wang, G. Ding, C. Zhang, X. Zhou, J. Yao, G. Cui and L. Chen, *Sci. Rep.*, 2014, **4**, 6472.
41. J. H. Kim, J. H. Kim, K. H. Choi, H. K. Yu, J. H. Kim, J. S. Lee and S. Y. Lee, *Nano Lett.*, 2014, **14**, 4438.
42. Y. C. Lu, B. M. Gallant, D. G. Kwabi, J. R. Harding, R. R. Mitchell, M. S. Whittingham and Y. Shao-Horn, *Energy Environ. Sci.*, 2013, **6**, 750.
43. K. S. Kang, Y. S. Meng, J. Breger, C. P. Grey and G. Ceder, *Science*, 2006, **311**, 977.
44. H. Chen, M. Armand, G. Demailly, F. Dolhem, P. Poizot and J. M. Tarascon, *ChemSuschem*, 2008, **1**, 348.
45. J. H. Kim, J. H. Kim, K. H. Choi, H. K. Yu, J. H. Kim, J. S. Lee and S. Y. Lee, *Nano Lett.*, 2014, **14**, 4438.
46. H. W. Lee, P. Muralidharan, C. M. Mari, R. Ruffo and D. K. Kim, *J. Power Sources*, 2011, **196**, 10712.
47. M. W. Jang, H.-G. Jung, B. Scrosati and Y.-K. Sun, *J. Power Sources*, 2012, **220**, 354.
48. M. Aklalouch, J. M. Amarilla, I. Saadoun and J. M. Rojo, *J. Power Sources*, 2011, **196**, 10222.
49. G. T. K. Fey, C. Z. Lu and T. P. Kumar, *J. Power Sources*, 2003, **115**, 332.
50. J. H. Cho, J. H. Park, M. H. Lee, H. K. Song and S. Y. Lee, *Energy Environ. Sci.*, 2012, **5**, 7124.
51. J. Liu, Q. Wang, B. Reeja-Jayan and A. Manthiram, *Electrochem. Commun.*, 2010, **12**, 750.
52. S. T. Myung, K. S. Lee, D. W. Kim, B. Scrosati and Y. K. Sun, *Energy Environ. Sci.*, 2011, **4**, 935.
53. W. Zhou, H. Gao and J. B. Goodenough, *Adv. Energy Mater.*, 2015, DOI: 10.1002/aenm.201501802.
54. W. Jiang, Z. Liu, Q. Kong, J. Yao, C. Zhang, P. Han and G. Cui, *Solid State Ionics*, 2013, **232**, 44.
55. J. Hassoun, R. Verrelli, P. Reale, S. Panero, G. Mariotto, S. Greenbaum and B. Scrosati, *J. Power Sources*, 2013, **229**, 117.
56. F. Croce, L. Settini and B. Scrosati, *Electrochem. Commun.*, 2006, **8**, 364.



### TOC

A novel kind of composite polymer electrolyte based on polytetrafluoroethylene supported poly(methylethyl  $\alpha$ -cyanoacrylate) is developed for  $\text{LiNi}_{0.5}\text{Mn}_{1.5}\text{O}_4$  /Li battery. A capacity retention (after 200<sup>th</sup> cycle) of  $\text{LiNi}_{0.5}\text{Mn}_{1.5}\text{O}_4$  /Li battery assembled with this composite polymer electrolyte is found to be 91.5 % at room temperature. Additionally, such composite polymer electrolyte presents comprehensive properties in high ionic conductivity, excellent thermal endurance, superior rate performance and longer cycling stability.